Chapter 1

Introduction

ZnO is a wide and direct bandgap semiconductor with experimental band gap energy of 3.4 eV. This material exists naturally as n-type whose conductivity is attributed to the existence of native point defects such as Zn interstitials and oxygen vacancies [1]. Impurities such as hydrogen [2, 3] which acts as a shallow donor and aluminium [4, 5] also contribute to the n-type conductivity of ZnO. As in other wide bandgap materials, there exists the so-called doping asymmetry, i.e. it is easy to obtain n-type ZnO but rather difficult to produce p-type ZnO. The existence of native defects in ZnO has hindered success in the fabrication of UV light emitting diodes because of their self-compensation behaviour [6].

ZnO possesses superior electronic and optoelectronic properties which make it a good candidate in optoelectronic, transparent electronics and spintronics applications. Its high efficiency in UV emission makes it a good material for fabrication of white lighting devices [7]. The resistance to radiation damage makes it possible to fabricate devices on ZnO that can operate within the UV region and in space applications, e.g. in solar cells as a transparent conducting oxide (TCO) [8], UV photodetectors, just to mention a few.

The use of ZnO in the fabrication of devices that can operate in space applications requires the devices to be highly stable, i.e. they must be resistant to high temperature fluctuations. Stable contacts on ZnO can be obtained through the use of metals with high melting points. The main problem with these types of contacts lies in the fabrication techniques to be used. With high melting point metals, the likely deposition techniques include among others, the electron-beam (e-beam) deposition and sputter deposition. However, these techniques tend to introduce defects in devices.

Defects are often detrimental to device operation. The use of ZnO in the fabrication of solar cells and UV detectors requires the material to be of high quality, i.e. with minimal defects as defects often influence the electrical and optical properties of semiconductors by affecting the doping, minority carrier lifetime and luminescence efficiency.

Apart from native point defects, ZnO also possesses deep level emission bands that emit all colours in the visible range with good colour rendering properties [9]. Knowledge and control of defects is essential to improve efficiency of devices; by removing them in the case of solar cell applications. Also, an understanding of the origins of emissions related to deep level defects in ZnO for development of highly efficient optoelectronic devices is required, i.e. to introduce them if necessary. Annealing of crystals is one possible way of recovering or removing defects in semiconductors. Defects can also be intentionally introduced in semiconductor material by irradiating with energetic particles.

Defect characterization in semiconductors is important for fabrication of high quality devices as it provides an understanding of the defect identity, defect control, properties and influence on devices. Different techniques have been used to characterize defects in semiconductors, some of which include the Hall Effect, positron annihilation spectroscopy (PAS), X-ray diffraction, Rutherford backscattering spectroscopy (RBS), admittance spectroscopy, cathodoluminescence and photoluminescence. In this thesis, deep level transient spectroscopy (DLTS) has been used to characterize deep level defects in ZnO.

DLTS is a capacitance based spectroscopic technique that can give information about the signature of an electrically active defect state, i.e. the activation enthalpy and capture cross-section within the bandgap of a semiconductor. This depletion layer method provides an environment where the occupancy of a deep state can be manipulated with relative ease [10, 11] by probing the depletion region of a metal/semiconductor contact, metal oxide semiconductor structure or an ordinary p-n junction.

An overview of the properties of ZnO as a semiconductor and its use in the fabrication of rectifying metal/semiconductor contacts is given in chapter 2. Chapter 3 gives an outline of defects in semiconductor materials with particular reference to ZnO. A method of characterizing defects in materials using capacitance based DLTS and Laplace-DLTS techniques is given in chapter 4. Experimental techniques employed in this particular work are outlined in chapter 5. Chapter 6 contains all the results and discussions obtained from this

work. A summary of conclusions drawn from the study are presented in chapter 7, while chapter 8 contains details of future studies to be carried out on ZnO.

References

1. D. C. Look, J. W. Hemsky and J. R. Sizelove, Phys. Rev. Lett. **82**, 2552 (1999)
2. D. G. Thomas and J. J. Lander, J. Chem. Phys. **25**, 1136 (1956)
3. E. Mollwo, Z. Phys. **138**, 478 (1954)
4. M. D. McCluskey and S. J. Jokela, Physica B, **401**, 355 (2007)
5. T. Minami MRS Bull. **25** (8), 38 (2000)
6. M. Willander, O. Nur, Q. X. Zhao, L. L. Yang, M. Lorenz, B. Q. Cao, J. Zuniga Perez, C. Czekalla, G. Zimmermann, M. Grundmann, A. Bakin, A. Behrends, M. Al-Suleiman, A. El-Shaer, A. C. Mofor, B. Postels, A. Waag, N. Boukos, A. Travlos, H. S. Kwack, G. Guinard, D. Si Le Dang, Nanotechnol. **20**, 332001 (2009)
7. A. Zainelabdin, S. Zaman, G. Amin, O. Nur, and M. Willander, Nanoscale Res. Lett. **5**, 1442 (2010)
8. A. Nuruddin, and J. R. Abelson, Thin Solid Films, **394**, 49 (2001)
9. M. Willander, O. Nur, N. Bano, K. Sultana, New J. Phys. **11**, 125020 (2009)
10. D. V. Lang, J. Appl. Phys. **45**, 7 (1974)
11. L. Dobaczewski, A. R. Peaker, K. Bonde Nielsen, J. Appl. Phys. **96**, 9 (2004)

Chapter 2

ZnO as a semiconductor

2.1 Introduction

ZnO is a wurtzitic compound semiconductor with a wide and direct bandgap of 3.4 eV at room temperature. This material occurs naturally as n-type with the native defects particularly zinc interstitials, and oxygen vacancies being proposed to be the source of n-type conductivity [1]. Some reports claim that the n-type conductivity is due to some impurities [2] introduced during material growth predominantly hydrogen and other group I related elements, arguing that the oxygen vacancy is too deep to contribute a significant concentration to the n-type conductivity of ZnO [3,4,5,6,7]. The effects of hydrogen in ZnO have been studied. It has been proposed that hydrogen in ZnO is a shallow donor [2,8,9] and can form several bond structures which include the BC_{II} and $BC_{\perp}$ configurations [2]. However the realization of *p*-type ZnO still remains a challenge as it lacks reproducibility [10, 11].

2.2 Crystal structure

ZnO is a highly ionic compound semiconductor which crystallizes into three common lattice structures, and these are; the rock salt, zinc blende and the wurtzite structure. The wurtzite structure is the most thermodynamically stable one at ambient conditions [12] i.e. for bulk ZnO crystals. This structure can be considered as two interpenetrating hexagonal-close-packed lattices, characterized by two interconnecting sublattices of Zn^{2+} and O^{2-} such that each Zn ion is surrounded by a tetrahedral of O ions and vice versa [13]. The tetrahedral arrangement gives rise to the polar symmetry along the hexagonal axis. Four common terminations for the wurtzitic ZnO structure exist and these are; Zn-polar terminated (0001)

and the O-polar terminated $(000\bar{1})$ faces (*c*-axis oriented), the non-polar $(11\bar{2}0)$ (a-axis) and $(10\bar{1}0)$ faces which both contain an equal number of Zn and O atoms. Due to the difference in face terminations, the polar faces have different physical and chemical structures; with the O-polar face having a unique electronic structure from the other three [13]. The wurtzite structure of ZnO is shown in Figure 2.1.

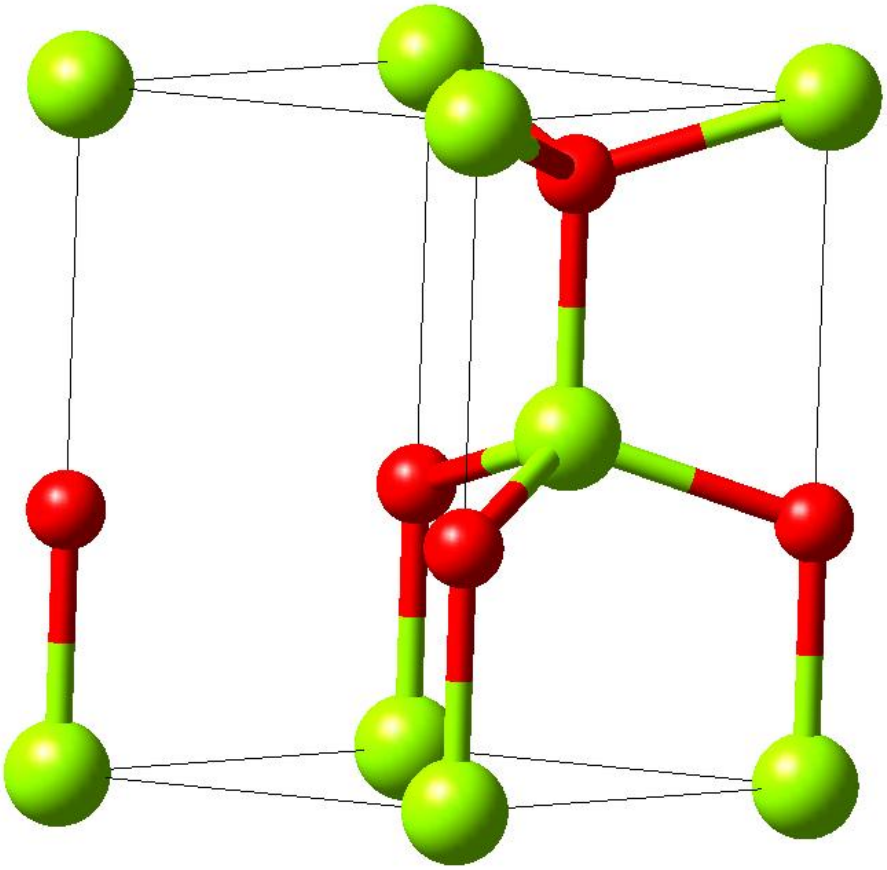

Figure 2.1: *The hexagonal wurtzite structure of ZnO. O atoms are shown as small dark spheres, Zn atoms as large light spheres. Redrawn from ref* [*14*].

The physical parameters of the wurtzite ZnO structure are given in Table 2.1.

Table 2.1: *Physical parameters of the wurtzite ZnO structure*

Parameter name	Symbol	Value	Temperature (K)	Ref
Lattice constants	a	3.249Å		[15]
	c	5.205Å		
Primitive lattice cell volume	V_{lc}	23.79Å^3		[15]
Electron affinity	χ	4.57 eV	300	[16]
Electron effective mass	m_e^*	0.27		[17]
Hole effective mass	m_h^*	0.59		[18]
Dielectric constants	ε_s^{II}	7.46		[19]
	$\varepsilon_s^{\perp}$	8.59		
Effective density of states	N_C	3.5×10^{18}cm^{-3}	300	[20]
	N_V	1.1×10^{19}cm^{-3}	300	

2.3 Material growth techniques

ZnO is available as bulk single crystals and also as thin films. Bulk material is grown using the hydrothermal, chemical vapour transport (CVT), and melt growth techniques, while thin film material is grown using the pulsed laser deposition, metalorganic chemical vapour deposition (MOCVD), metalorganic vapour phase epitaxy (MOVPE), just to mention a few. In this particular study, main focus is on melt grown bulk ZnO single crystals. Traditional melt growth processes rely on material growth from a melt or liquid. They are associated with three main hindrances, which include melt containment, ZnO decomposition at atmospheric pressure near the melting point, and crystal contamination [21]. These problems are however eliminated in the melt growth technique used by Cermet [21]. The melt growth technique produces high quality material that is free from solvent related impurities and thus minimal defects. The other advantage of this technique is the high material growth rate [21].

2.4 Properties and Applications

Due to its wide bandgap, this material finds its use in several applications some of which include the fabrication of ultraviolet detectors and daylight-blind UV detectors, transparent conducting oxides, acoustic wave devices, light emitting diodes, laser diodes, high frequency electronic devices, varistors, piezoelectric transducers, and paints. ZnO has an excitonic binding energy of 60 meV at room temperature and is compatible with the conventional chemistry etching similar to that used in Si technology which gives it more advantages over other wide band gap materials, e.g. GaN.

The use of ZnO in the electronic and optoelectronic industries requires the fabrication of highly stable good quality metal/ZnO contacts. Fabrication of good quality rectifying contacts has been a problem since the early discoveries of the material and still remains a challenge as different Schottky barrier heights have been reported for the same metal deposited on ZnO. Reports have indicated the dependence of contact quality on cleaning procedures used other than on the metal work function [22]. Polarity of the material [23] (in the case of bulk material) and the deposition techniques used [24] have also been reported to affect contact quality. This is valid since different cleaning procedures will influence the surface states, hydrocarbon and hydroxide surface contamination, oxygen chemisorption, subsurface defects and surface morphology due to the chemical reactions taking place at the surface. The above-mentioned will in turn affect the metal-surface reactions and hence the contact quality.

Table 2.2 shows the variation of measured current voltage (IV) parameters with cleaning procedures and deposition techniques from selected references. These parameters have been obtained at room temperature.

Table 2.2: *Values of barrier height, ideality factor and degree of rectification* (*defined as the ratio of the forward current to the reverse current at 1.0V*) *from selected references.*

Growth Technique	Cleaning Procedure	Deposition Technique	Metal (ZnO-face)	Barrier Height(eV)	Ideality factor	Degree of Rectification	Ref
hydrothermal	OS	e-beam	Pd(O-polar)	0.75	1.4	~2	[25]
Melt	OSA	e-beam	Pd(Zn-polar)	0.55	2.0	~2	[23]
Melt	OSA	e-beam	Pd(O-polar)	0.59	1.2	~4	[23]
Melt	OSA	e-beam	Pt(Zn-polar)	0.55	2.0	~2	[23]
Melt	OSA	e-beam	Pt(O-polar)	0.68	1.2	~4	[23]
Melt	OSA	resistive	Au(Zn-polar)	0.71	1.4	~5	[23]
Melt	OSA	resistive	Au(O-polar)	0.69	1.1	~5	[23]
Melt	OSA	resistive	Ag(Zn-polar)	0.78	1.2	~7	[23]
Melt	OSA	resistive	Ag(Zn-polar)	0.77	1.1	~7	[23]
Melt	OSP	resistive	Au(Zn-polar)	0.63	1.15	~4	[26]
MOCVD	OSP	-	Pt(--)	0.78	1.02	~6	[27]
Hydrothermal	OSA	sputter	Pt(Zn-polar)	0.96	1.1	~6	[28]
Hydrothermal	OSA	sputter	Pt(O-polar)	0.60	3.1	~2	[28]
PLD	OSA, RP	--	Pd(11$\underline{2}$0)	0.68	1.4	~4	[29]
PLD	OSA, RP	--	Ag(11$\underline{2}$0)	0.59	1.4	-	[29]
Hydrothermal	ROP	e-beam	Ir(O-polar)	0.64	1.36	~4	[30]
Melt	OSP	resistive	Pd(O-polar)	0.77	1.85	~8	[31]
Melt	OSP	resistive	Pd(Zn-Polar)	0.72	1.43	~8	[34]
Melt	OSP	e-beam	Pd(Zn-Polar)	0.62	1.66	~5	[34]

* Organic solvents only, (OS), organic solvents and any acid etch (OSA), organic solvent and hydrogen peroxide treatment (OSP), Remotely oxygen plasma cleaned (ROP), remotely plasma cleaned (RP).

A dramatic improvement of contact quality has been reported after the treatment of the material with hydrogen peroxide [26,27,32,33,34,35]. The study of the effects of deposition techniques has not been extensively carried out. High quality metal/ZnO contacts are of importance in the fabrication of UV detectors and also in the characterization of deep level defects in semiconductors.

Modifications of the electrical properties of ZnO after annealing in different ambient conditions have been studied using Hall Effect measurements [36,37,38], photoluminescence [39] and DLTS measurements [40,41,42]. The Hall Effect measurements have indicated an increase in surface conductivity after hydrogen annealing [43, 44] which influences device characteristics. A reduction of the shallow donor concentration in ZnO after Ar annealing has been reported [45]. Passivation of deep level defects in ZnO after hydrogen annealing has also been observed using the PL measurements [44]. Oxygen annealing at high temperatures is also of very high significance as it helps in eliminating surface adsorbents. At the same time, it leads to surface thermal decomposition which is an ideal method for preparing the material for surface electronic studies. This clearly indicates that the electronic and optical properties of ZnO can be easily altered by thermal treatments to suit the needs of the researcher. The fact that ZnO allows for band gap engineering by alloying it with MgO and CdO to increase and decrease its bandgap energy, respectively [46] is an important aspect since it allows for tuning of the material's optoelectronic properties for use in selected wavelengths of the electromagnetic spectrum for selective light sensing purposes.

2.5 Metal/ZnO contacts

2.5.1 Introduction

Metal/semiconductor contacts are important to the microelectronics industry as well as in the characterization of fundamental properties of semiconductors using junction techniques e.g. DLTS. The quality of a metal/semiconductor contact determines its performance as poor contacts result in undesired effects e.g. high leakage currents and low barrier heights. Metal/semiconductor quality is determined by a number of factors, some of which include the mismatch between the Fermi-energies of the metal and semiconductor, the semiconductor processing steps (cleaning and annealing) prior to contact fabrication and the contact fabrication techniques. These contacts are considered to be ohmic or rectifying (Schottky) as governed by their response to an applied external bias.

2.5.2 Ohmic contacts

A contact is said to be ohmic if the barrier formed from the intimate contact of a metal and semiconductor is zero. In an ideal ohmic contact, charge carriers are free to move in either direction across the contact with minimal or no resistance. To fabricate such a contact on an n-type semiconductor, we require that the metal work function must be closer to or smaller than the semiconductor electron affinity. Formation of such a contact is illustrated in Figure 2.2.

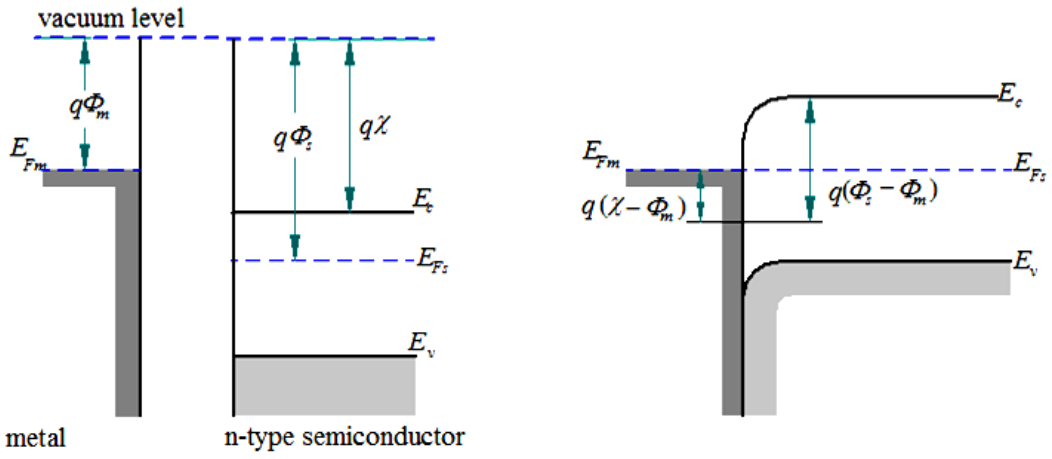

(a) (b)

Figure 2.2: Ohmic contacts to n-type semiconductor $\Phi_M < \Phi_S$ (*a*) *before contact,* (*b*) *equilibrium band diagram for the contact. Adopted from ref* [14]

Bringing the metal into intimate contact with the semiconductor will result in Fermi-level alignment as shown in Figure 2.2b. This raises the semiconductor electron energies relative to the metal, reducing the barrier to electron flow between the metal and semiconductor. However under real situations, ohmic contact formation is affected by external factors, some of which include; conditions under which the contacts are fabricated, surface states, interface states, and also reactions between the metal and semiconductor. Ohmic contacts are classified into tunnel, and annealed and alloyed contacts; with the tunnel contacts being the most practical ones. Tunnel contacts possess a positive barrier at the metal/semiconductor interface, but also have enough doping in the semiconductor such that there is only a thin barrier separating the metal from the semiconductor. This thin barrier allows carriers to easily tunnel through the interface. For an ohmic contact, under any applied biasing conditions, the IV characteristics must always obey Ohm's law, since there is a very thin barrier for electron flow in any given direction, i.e. metal to semiconductor or semiconductor to metal.

2.5.3 Schottky contacts

If a metal-semiconductor contact can rectify signals in the forward biased mode and allows negligible or no current to flow in the reverse bias, it is referred to as a Schottky contact. Ideal Schottky contacts are formed when a difference in potential exists between the Fermi energy of the metal and the band edge where majority charge carriers reside (ignoring the effects of surface and interface states). The formation of a Schottky contact is illustrated in Figure 2.3. The difference in potential between the Fermi-energy of the metal and semiconductor gives the barrier height, ϕ_B. For an n-type semiconductor, the barrier height is given theoretically as [47];

$$\phi_B = \phi_M - \chi_S \qquad (2.1)$$

where ϕ_M is the metal work function, χ_S is the electron affinity of the semiconductor. In real Schottky contacts, the barrier height is affected by interfacial layers, surface states, defects and chemical reactions which also determine the quality of the contacts.

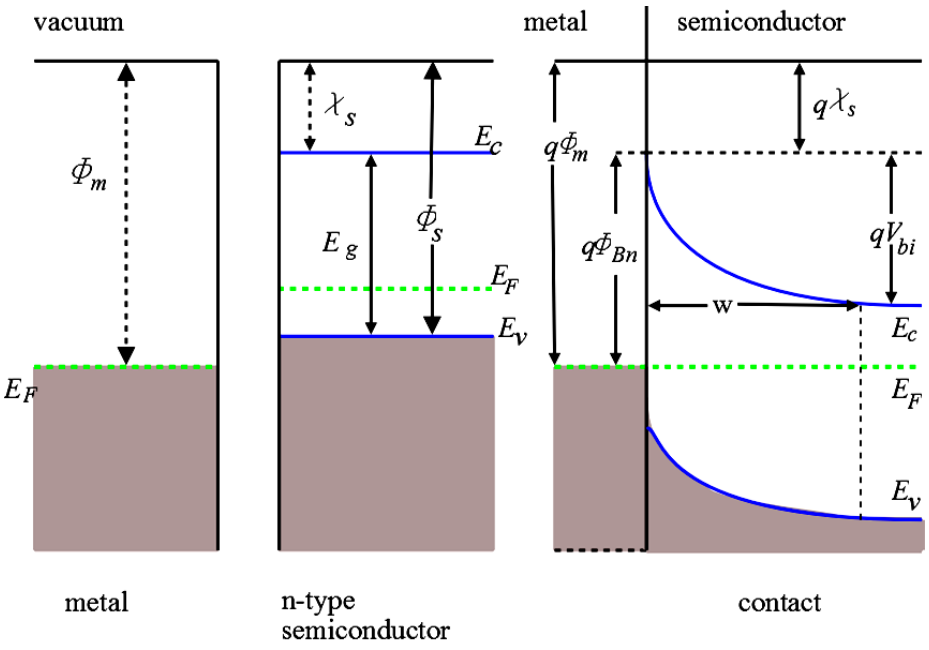

Figure. 2.3: Flatband diagram of a metal/n-type semiconductor contact at equilibrium. Redrawn after ref [14]

2.5.3.1 Current-voltage (IV) measurements

The current voltage technique offers a good method for evaluating the quality of a Schottky contact by determining the reverse and forward current that flows through the device under different biasing conditions. This enables us to deduce the current transport mechanisms that dominate the conduction process within the device. Figures of merit which include barrier height, ideality factor and series resistance can also be obtained.

In this section, a couple of IV characteristics obtained from metal/ZnO structures are presented and discussed. This section aims to point out some of the factors affecting the quality of the contacts, in as much as the fabrication techniques and material processing steps are concerned.

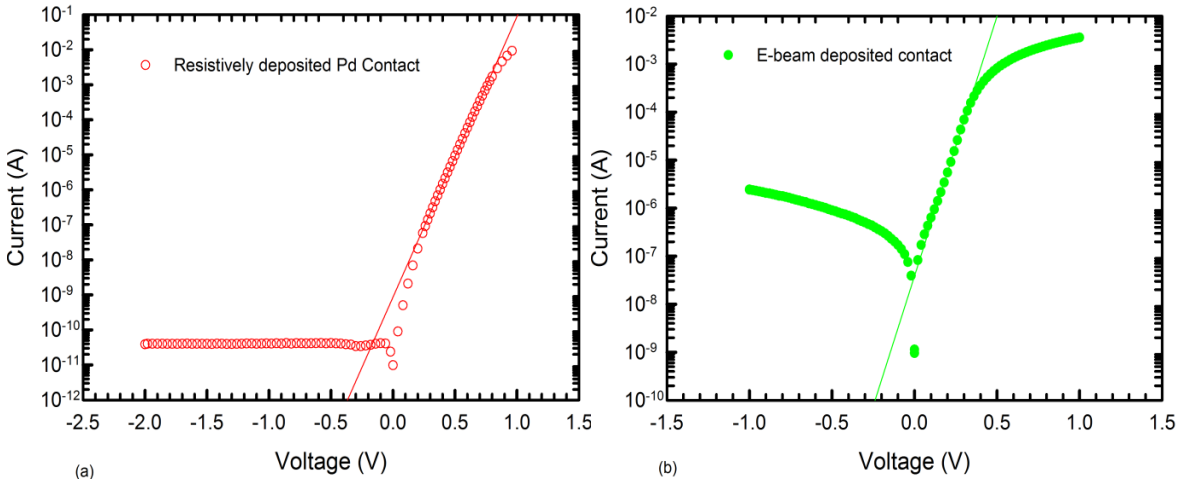

Figure 2.4: *A semi-logarithmic IV characteristics of (a) resistively deposited and (b) e-beam deposited Pd/ZnO Schottky contacts obtained at 298 K from the best selected contacts.*

A typical current-voltage characteristic of metal/ZnO Schottky contacts is illustrated in Figure 2.4. These contacts show a strong dependence on the contact fabrication technique used since the material processing steps are the same. The straight line shows the linear fit to the data by assuming a pure thermionic emission model. The current flowing through the metal semiconductor contact is given by [48],

$$I = I_S \exp\left[\frac{q(V - IR_s)}{nkT}\right]\left\{1 - \exp\left[\frac{q(V - IR_s)}{kT}\right]\right\} \qquad (2.2)$$

where V is the applied voltage, R_s is the series resistance, n is the ideality factor, I_s is the saturation current. From the straight line fit shown in Figure 2.4, the ideality factor and the barrier height can be deduced. The ideality factor is obtained from the gradient, as,

$$n = \frac{q}{2.3kT \cdot [d(\ln I)/dV]} = \frac{q}{2.3mkT} \qquad (2.3)$$

where m is the gradient of the straight line. The saturation current is obtained as the intercept to the $\ln I$ axis at $V = 0$ as,

$$I_S = AA^*T^2 \exp\left(-\frac{q\phi_B}{kT}\right) \qquad (2.4)$$

where A is the Schottky contact cross-sectional area, A^* is the Richardson constant, T is the temperature in Kelvin, k is the Boltzmann constant and ϕ_B is the barrier height calculated as

$$\phi_B = \frac{kT}{q} \ln\left[\frac{AA^*T^2}{I_S}\right] \qquad (2.5)$$

Deviations from linearity at high applied voltage are due to the effects of series resistance. The resistive evaporation technique proves to produce better quality contacts with very low leakage currents and a higher degree of rectification compared to the e-beam deposited contacts. Table 2.3 shows some of the parameters extracted from the resistively deposited and e-beam deposited contacts by fitting the data to a pure thermionic emission model.

Table 2.3: *Values of ideality factor n, Schottky barrier height (SBH), series resistance, saturation current I_s and the degree of rectification for the resistively and electron-beam (E-beam) deposited Pd contacts.*

Deposition Technique	Ideality factor, *n*	SBH (eV)	Series Resistance (Ω)	Saturation current, I_s (A)	*Degree of rectification
Resistive	1.56 ± 0.05	0.75 ± 0.01	21 ± 5	$(1.1 \pm 0.4)\times10^{-10}$	9
E-Beam	1.7 ± 0.2	0.60 ± 0.02	143 ± 7	$(8.4 \pm 5)\times10^{-8}$	3

*Refers to the ratio of the forward current measure at 1.0 V to the reverse current at 1.0 V

From the average parameters shown in Table 2.3, it can be observed that the resistive technique yields better quality contacts compared to the e-beam technique. However, it must be noted that in some cases it is not a matter of choice for one not to use the latter technique. To fabricate contacts which are thermally stable at high temperatures, high melting point metals must be used. Since these metals cannot be resistively evaporated, other techniques e.g. sputter deposition or e-beam deposition must be employed. IV characteristics of some chosen high melting point metals are shown in Figure 2.5.

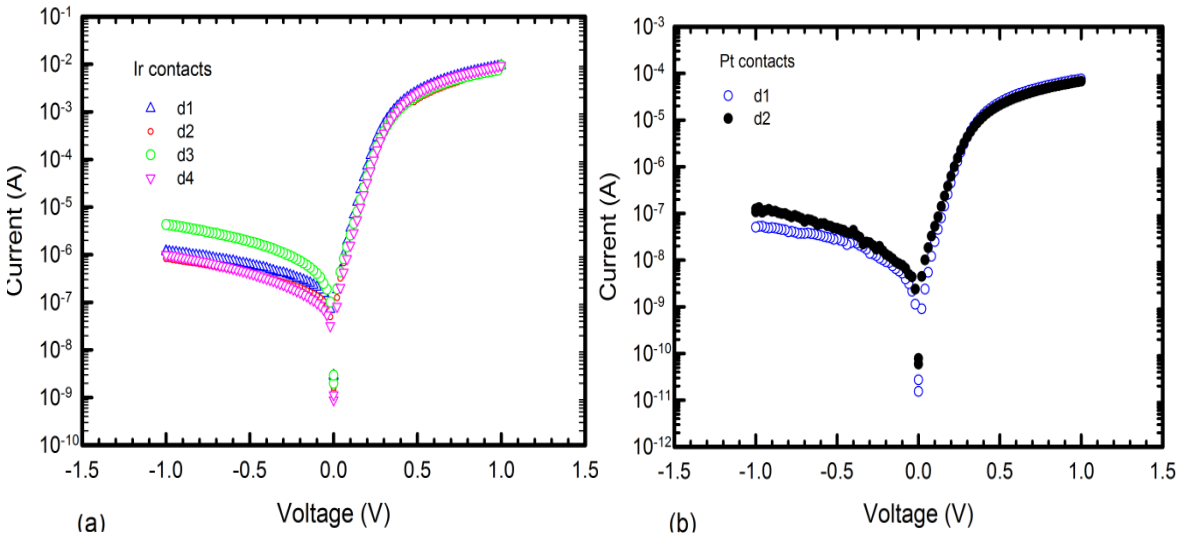

Figure 2.5: *Semi-logarithmic IV characteristics of (a) Ir and (b) Pt contacts obtained at 298 K.*

Table 2.4: *Values of ideality factor n, Schottky barrier height (SBH), series resistance, saturation current I_s and the degree of rectification for the electron-beam (e-beam) deposited Ir and Pt contacts.*

Metal	Ideality factor, *n*	SBH (eV)	Series Resistance (Ω)	Saturation current, I_s (A)	Degree of rectification
Ir	1.29 ± 0.02	0.567±0.003	77 ± 7	$(1.2 \pm 0.1)\times10^{-7}$	5
Pt	1.5 ± 0.1	0.67 ± 0.01	$(9 \pm 0.3)\times10^{3}$	$(3 \pm 1)\times10^{-9}$	3

For all the characteristics presented in this chapter, the e-beam deposited contacts have poor quality contacts in terms of leakage current and lower orders of rectification compared to the resistively deposited contacts. This has been attributed to the damage caused by the ionized gas particles that impinge onto the sample causing damage to the surface. Since the filament is not a true point source of electrons; stray electrons originating from it and are not focused onto the metal can also impinge onto the sample [49].

Annealing of samples prior to contact fabrication and after fabrication also affects the quality of the contacts. This is because annealing can recover defects in crystals or can remove defects which in turn affect device operation. Figure 2.6 shows some IV characteristics of metal contacts fabricated on ZnO samples annealed at different temperatures. It must be mentioned that the ZnO samples were first annealed in Ar at different temperatures prior to contact fabrication. This is because annealing of the samples at elevated temperatures with the Schottky contacts fabricated would result in an ohmic behaviour as has been observed by Mtangi *et al*. [31] on Pd/ZnO structures annealed in Ar.

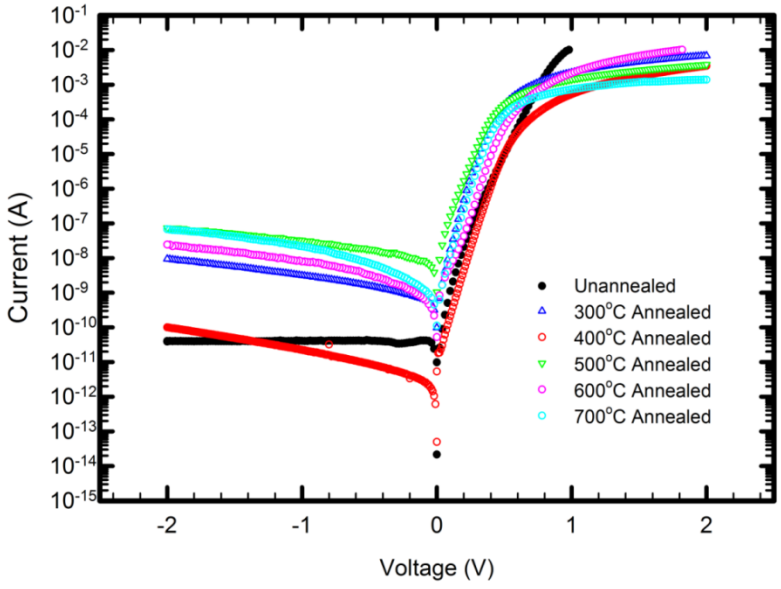

Figure 2.6: *Semi-logarithmic IV plots of the Pd/ZnO devices obtained at 298 K.*

The other reason for annealing the samples prior to contact fabrication is to avoid the modification of the depletion region of the metal semiconductor contact through in diffusion of the metal into the semiconductor or by vice-versa and also the formation of metal/Zn eutectics. It can be observed that the annealed contacts show an increased reverse current at -2.0 V as compared to the un-annealed contacts. A possible explanation for such an increase in reverse current could be the modification of the layer closer to the surface with annealing, which becomes highly conductive where the surface electrons can contribute to the current through surface conduction as has been suggested [38]. Another possibility is that, annealing can introduce subsurface and also deep level defects that can assist carriers in tunnelling through the barrier increasing the reverse current. Annealing of samples is significant as it can cause thermal decomposition of the ZnO surface (particularly in O_2) which can be used for surface electronic studies of the material [50].

Figure 2.7 shows the IV characteristics of Pt/ZnO Schottky contacts annealed in (a) Ar and (b) O_2, respectively.

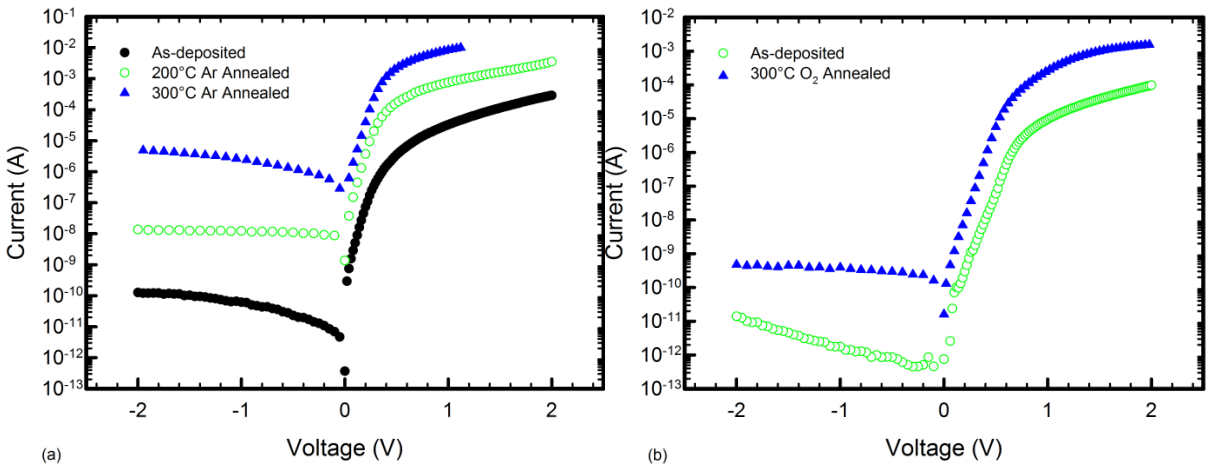

Figure 2.7: *Semi-logarithmic IV characteristics of Pt/ZnO Schottky contacts annealed in (a) Ar and (b) oxygen ambient*.

From these characteristics, an increase in reverse current is observed after annealing the contacts. The series resistance effects are also reduced. Interesting enough, for samples annealed prior to contact fabrication (Figure 2.6), the series resistance effects are increased. This is possibly due to some accumulation of surface adsorbents during annealing. For samples annealed with contacts fabricated (Figure 2.7), the decrease in series resistance can possibly due to the reduction in the concentration of surface and/or interface states density

because of the solid state reaction which might occur between the metal and semiconductor during annealing. The ideality factor, the series resistance and barrier height obtained from the best selected contacts are shown in Table 2.5.

Table 2.5: *Values of ideality factor, SBH, series resistance and degree of rectification obtained from the best selected Pt/ZnO contacts.*

Annealing ambient	Annealing Temperature (°C)	Ideality factor, *n*	SBH (eV)	Series Resistance (Ω)	Degree of rectification
------	----------	1.53	0.72	2.69k	7
Ar	200	1.50	0.62	0.48k	5
Ar	300	1.64	0.55	71	4
------	-------	2.14	0.82	11.8k	7
O_2	300	1.84	0.75	0.61k	6

The barrier height decreases with increase in annealing temperature as carriers can now easily cross over the barrier. The series resistance however is drastically reduced for the Ar annealed samples. The same is also observed for the O_2 annealed contacts. However, there is a decrease in the order of rectification with annealing. Thus annealing can also have an effect on the quality of contacts.

2.5.3.2 Capacitance-voltage (CV) measurements

An understanding of the impurity distribution in semiconductor material is essential in the fabrication of devices. The CV technique is ideal to help bring this understanding by analysing the depletion region of a semiconductor through the CV profiling method. This method makes use of the differential capacitance. Under reverse bias conditions, the width of the space charge region of a metal/semiconductor junction depends on the applied voltage. Superimposing a small ac signal upon dc bias results in a separation of negative charges from positive charges where the metal assumes more negative charge which induces a positive charge within the semiconductor region. This creates a region depleted of charge carriers called the depletion region. This junction resembles a parallel plate capacitor with the depletion region acting as a dielectric. A typical CV characteristic is shown in Figure 2.8.

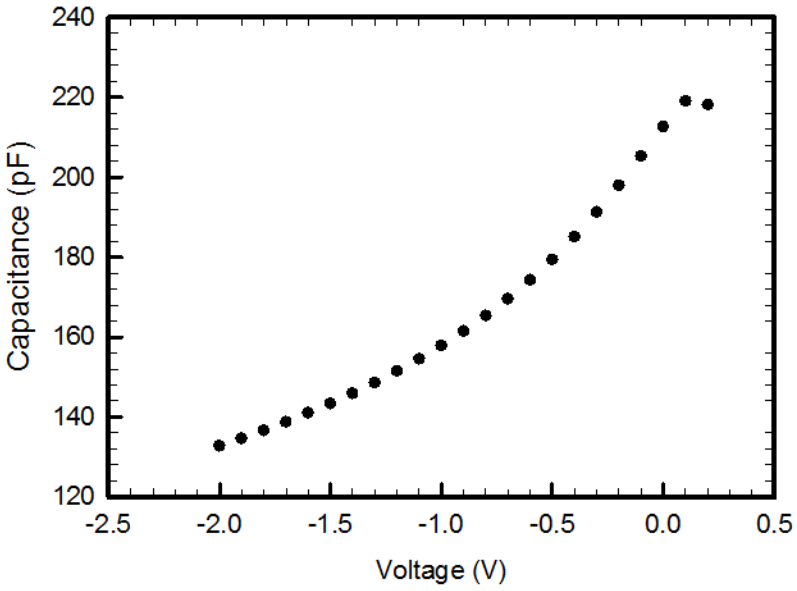

Figure 2.8: *Room temperature CV characteristics obtained from a Pd/ZnO Schottky contact annealed at 400*°C *in Ar.*

2.5.4 The Depletion layer

Based on the depletion width approximation, the semiconductor is assumed to be divided into two distinct regions. These are a layer closer to the interface which is completely depleted of charge carriers and an interior region of perfect charge neutrality in which no electric field exists. The charge density $\rho(x)$ in the depletion region where there are no electrons in the conduction band is given by qN_D. If the depletion width is w, the charge density in the semiconductor can be written as [47,51]:

$$\rho(x) = \begin{cases} qN_D & \text{if } x \leq w \\ 0 & \text{if } x > w \end{cases} \qquad (2.6)$$

where N_D is the dopant density and q is the electronic charge.

The existence of an electric field due to charge separation results in a potential difference to across the metal-semiconductor junction. The shape of the band edge profiles can be determined by solving Poisson's equation and applying the necessary boundary conditions. These boundary conditions are obtained from:

(a). the barrier height

(b). the electric field; considering it to be zero within the bulk of the semiconductor.

Taking x to be zero at the interface, $x = 0$ the boundary conditions can be written as $V(0) = V_d$

and $E(\infty) = 0$. The solution for the Poisson's equation can be written in one-dimension as

$$\frac{d^2V}{dx^2} = \frac{1}{\varepsilon_s}\rho(x) \tag{2.7}$$

where $\rho(x)$ is the total charge density in the semiconductor at a depth x and ε_s is the semiconductor permittivity. If $\rho(x)$ includes contributions from the valence band, conduction band, ionized donors and acceptors, the resulting equation becomes more complicated and would require numerical methods to solve it. Making use of the depletion width approximation, integrating equation (2.7) twice and applying the boundary conditions will give the depletion layer width as [42],

$$w = \sqrt{\frac{2\varepsilon_s V_{\mathrm{d}}}{qN_{\mathrm{D}}}} \tag{2.8}$$

Under an externally applied bias, V_a the depletion region is given by,

$$w = \sqrt{\frac{2\varepsilon_{\mathrm{s}}}{qN_{\mathrm{D}}}\left(V_{\mathrm{bi}} - V_a - \frac{kT}{q}\right)} \tag{2.9}$$

The electric field in the semiconductor is also given by,

$$E(x) = -\frac{qN_{\mathrm{D}}}{\varepsilon_{\mathrm{s}}}(w - x) \tag{2.10}$$

The electrostatic potential can be obtained by integrating equation (2.10) as

$$V(x) = -\frac{qN_{\mathrm{D}}}{\varepsilon_{\mathrm{s}}}\left(wx - \frac{1}{2}x^2\right) \tag{2.11}$$

The space charge per unit area of the semiconductor, Q_{sc} is given by

$$Q_{\mathrm{sc}} = qN_D w = \sqrt{2\varepsilon_{\mathrm{s}} qN_{\mathrm{D}}\left(V_{\mathrm{bi}} - V_a - \frac{kT}{q}\right)} \tag{2.12}$$

If this is the amount by which the charge within the depletion width w changes due to a dc bias, then a differential or small signal capacitance is given by,

$$C = \frac{|\partial Q_{\mathrm{sc}}|}{\partial V_a} = \sqrt{\frac{\varepsilon_s qN_{\mathrm{D}}}{2(V_{\mathrm{bi}} - V_a - kT/q)}} = \frac{\varepsilon_{\mathrm{s}} A}{w} \tag{2.13}$$

This can be written in the form,

$$\frac{1}{C^2} = \frac{2(V_{\text{bi}} - V_a - kT/q)}{\varepsilon_s A^2 q N_{\text{D}}} \tag{2.14}$$

A plot of $1/C^2$ *versus* V_a yields a straight line where the doping density, N_{D} can be calculated from the gradient provided N_{D} is constant throughout the depletion region. The built-in-voltage, V_{bi} is obtained from the voltage intercept. The net doping density is given by;

$$N_{\text{D}} = \frac{2}{A^2 q \varepsilon_s}\left\{-\frac{1}{d(1/C^2)/dV}\right\} \tag{2.15}$$

Figure 2.9 shows a typical $1/C^2$ *versus* V_a plot.

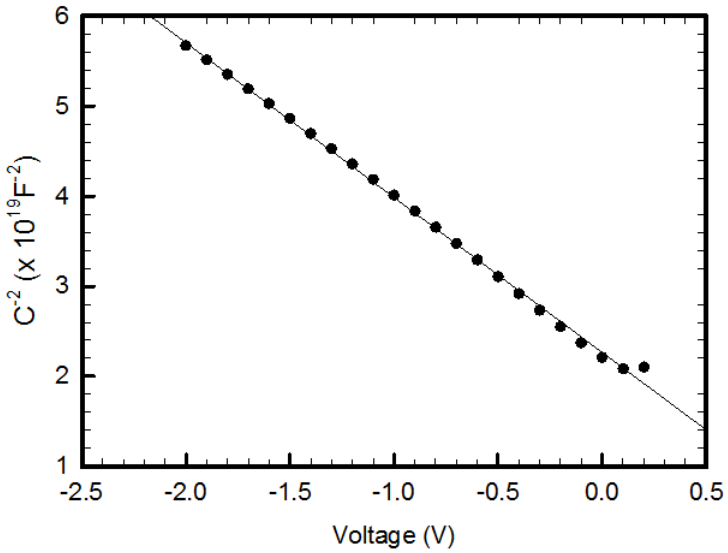

Figure 2.9: *Room temperature* $1/C^2$ *versus* V_a *characteristics obtained from a Pd/ZnO Schottky contact annealed at 400*°C *in Ar.*

By varying the depletion region width through changing the applied voltage and measuring the capacitance, the net doping profile of the semiconductor can be obtained using equation (2.14). A typical net doping profile is shown in Figure 2.10.

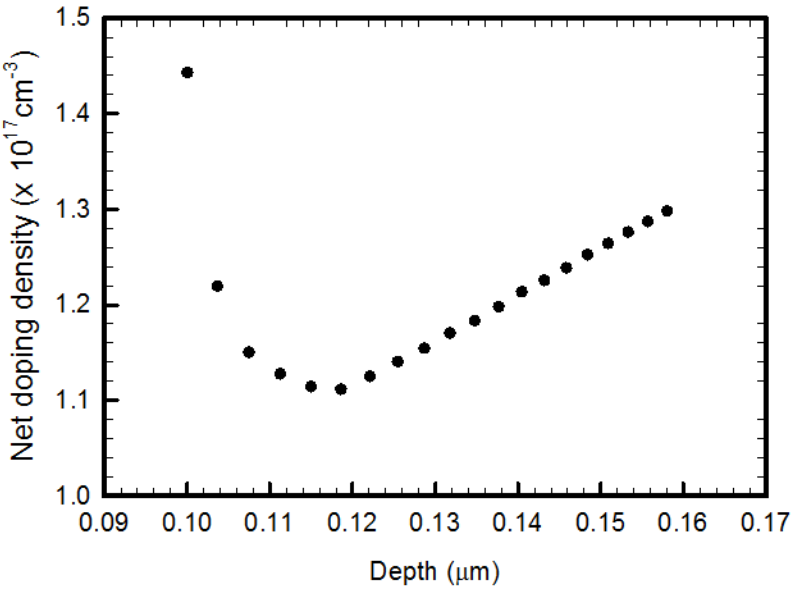

Figure 2.10: *Net doping profile of the Pd/ZnO Schottky contact annealed at 400*°C *in Ar*.

As indicated in Figure 2.10, 400°C Ar annealed ZnO sample reveal a concentration gradient towards the surface. A region up to a depth of 0.16 μm below the metal/semiconductor interface has been probed at a reverse bias of 2.0 V.

Summary

From Table 2.2 and the *IV* characteristics presented in this chapter, it can be mentioned that processing steps prior to Schottky contact fabrication and the deposition techniques used affect the quality of the semiconductor devices. This can be explained by the fact that different cleaning techniques and chemicals react differently with ZnO. As a result of these differences, different surface morphologies, surface states, subsurface defects and chemical reactions influence the quality of the contacts formed. These factors cause a variation of barrier heights obtained from metal/ZnO structures even with the same metal being used. This shows that Schottky contact fabrication on ZnO still needs further investigations to fully understand these structures. The barrier heights determined from these particular contacts vary from $0.55 - 0.96$ eV. The resistive evaporation technique produces contacts with very low reverse currents and higher degrees of rectification. E-beam deposition as well as annealing of the samples prior to contact fabrication seems to increase the reverse current that flows through the contacts. The possible explanation for such behaviour could be an introduction of defects within semiconductor material that can promote recombination and other current transport mechanisms other than pure thermionic emission. An investigation into the defects that might have been possibly introduced into the semiconductor material during fabrication and processing is to be performed using DLTS and high resolution Laplace DLTS.

References

1. D. C. Look, J. W. Hemsky and J. R. Sizelove, Phys. Rev. Lett. **82**, 2552 (1999)
2. C. G. Van de Walle, Phys. Rev. Lett. **85**, 5 (2000)
3. E. C. Lee, Y-S. Kim, Y.-G. Jin, and K. J. Chang, Phys. Rev. B **64**, 085120 (2001)
4. S. B. Zhang, S. H. Wei, and A. Zunger, Phys. Rev. B, **63**, 075205 (2001)
5. A. F. Kohan, G. Ceder, D. Morgan, and C. G. Van de Walle, Phys. Rev. B **61**, 15019 (2000)
6. F. Oba et al., J. Appl. Phys. **90**, 824 (2001)
7. A. Janotti and C. G Van de Walle, Appl. Phys. Lett. **87**, 122102 (2005)
8. D. G. Thomas, and J. J. Lander, J. Chem. Phys. **25**, 1136 (1956)
9. E. V. Lavrov, J. Weber, F. Borrnert, C. G. Van de Walle, and R. Helbig, Phys. Rev. B. **66**, 165205 (2002)
10. B. Yao, D. Z. Shen, Z. Z. Zhang, X. H. Wang, Z. P. Wei, B. H. Li, Y. M. Lv, X. W. Fan, L. X. Guan, G. Z. Xing, C. X. Cong, and Y. P. Xie, J. Appl. Phys. **99**, 123510 (2006)
11. M. D. McCluskey and S. J. Jokela, J. Appl. Phys. **106**, 071101 (2009)
12. U. Özgür, A comprehensive review of ZnO materials and devices, J. Appl. Phys. **98**, 41301 (2005)
13. C. Jagadish and J. Pearton, Zinc Oxide Bulk, Thin Films and Nanostructures Processing, Properties and Applications, Elsevier, Oxford, UK, Amsterdam, Netherlands, (2006)
14. W. Mtangi, MSc Dissertation, University of Pretoria 2009
15. R.B. Heller, J. McGannon, and A.H. Weber. Precision determination of the lattice constants of zinc oxide. J. Appl. Phys., **21**, 1283 (1950)
16. R.K. Swank. Surface properties of II-VI compounds. Phys. Rev. **153**, 844 (1967)
17. W.S. Baer. Faraday rotation in ZnO: Determination of the electron effective mass. Phys. Rev. **154**, 785 (1967)
18. M. Oshikiri, Y. Imanaka, F. Aryasetiawana and G. Kido, Physica B, **298**, 472 (2001)
19. N. Ashkenov, B.N. Mbenkum, C. Bundesmann, V. Riede, M. Lorenz, D. Spemann, E.M. Kaidashev, A. Kasic, M. Schubert, M. Grundmann, G.Wagner, H. Neumann, V. Darakchieva, H. Arwin, and B. Monemar. Infrared dielectric functions and phonon modes of high-quality ZnO films. J. Appl. Phys. **93**, 127 (2003)
20. M. Schmidt, PhD Thesis, Leipzig University, 2012
21. http://www.cermetinc.com/materials/crystal_growth.htm, 24/07/2012
22. A. Y. Polyakov, N. B. Smirnov, E. A. Kozhukhova, V. I. Vdovin, K. Ip, Y. W. Heo, D. P.

Norton, and S. J. Pearton, Appl. Phys. Lett. **83**, 1575 (2003)

23. M. W. Allen, M. M. Alkaisi, and S. M. Durbin, Appl. Phys. Lett. **89**, 103520 (2006)
24. W. Mtangi, F. D. Auret, P. J. Janse van Rensburg, S. M. M. Coelho, M. J. Legodi, J. M. Nel, W. E. Meyer, and A. Chawanda, Appl. Phys. Lett. **110**, 094504 (2011)
25. U. Grossner, S. Gabrielsen, T. M. Børseth, J. Grillenberger, A. Y. Kuznetsov, and B. G. Svensson, Appl. Phys. Lett. **85**, 2259 (2004)
26. Q. L. Gu, C. K. Cheung, C. C. Ling, A. M. C. Ng, A. B. Djuriˆsiæ, L. W. Lu, X. D. Chen, S. Fung, C. D. Beling, and H. C. Ong, J. Appl. Phys. **103**, 093706 (2008)
27. A. Nakamura, and J. Temmyo, J. Appl. Phys. **109**, 093517 (2011)
28. H. Endo, M. Sugibuchi, K. Takahashi, S. Goto, S. Sugimura, K. Hane, and Y. Kashiwaba, Appl. Phys. Lett. **90**, 121906 (2007)
29. H. von. Wenckstern, E. M. Kaidashev, M. Lorenz, H. Hochmuth, G. Biehne, J. Lenzner, V. Gottschalch, R. Pickenhain, and M. Grundmann, Appl. Phys. Lett. **84**, 79 (2004)
30. L. J. Brillson, H. L. Mosbacker, M. J. Hetzer, Y. Strzhemechny, G. H. Jessen, D. C. Look, G. Cantwell, J. Zhang, and J. J. Song, Appl. Phys. Lett. **90**, 102116 (2007)
31. W. Mtangi, F.D. Auret, A. Chawanda, P.J. Janse van Rensburg, S.M.M. Coelho, J.M. Nel, M. Diale, L. van Schalkwyk, C. Nyamhere, Materials Science and Engineering B **177**, 180 (2012)
32. R. Schifano, E. V. Monakhov, U. Grossner, and B. G. Svensson, Appl. Phys. Lett. **91**, 193507 (2007)
33. C. H. Tsai, S.-X. Lin, C. I. Hung, C. C. Liu, and M. P. Houng, J. Appl. Phys. **106**, 093702 (2009).
34. S. H. Kim, H. K. Kim, and T. Y. Seong, Appl. Phys. Lett. **86**, 112101 (2005)
35. W. Mtangi, F.D. Auret, C. Nyamhere, P.J. Janse van Rensburg, M. Diale, A. Chawanda, Phys. B. **404**, 1092 (2009)
36. D.C. Look, Superlattices Microstruct., **42**, 284 (2007)
37. G.H. Kassier, M. Hayes, F.D. Auret, M. Diale, B.G. Svensson, Phys. Status Solidi C **5**, 569 (2008)
38. W. Mtangi, J.M. Nel, F.D. Auret, A. Chawanda, M. Diale and C. Nyamhere, Physica B **407**, 1624 (2011)
39. D. C. Look, G. C. Farlow, P Reunchan, S Limpijumnong, S. B. Zhang, and K. Nordlund, Phys. Rev. Lett. **95**, 225502 (2005)
40. H. von Wenckstern, G. Biehne, M. Lorenz, M. Grundmann, F. D. Auret, W. E. Meyer, P. J. Janse van Rensburg, M. Hayes, J. M. Nel, J. Kor. Phys. Soc. **53**, 5 (2008)

41. V. Quemener, L. Vines, E. V. Monakhov, B. G. Svensson, Int. J. Appl. Ceram. Technol. **8**, 5 1017 (2011)
42. D. M. Hofmann, D. Pfisterer, J. Sann, B. K. Meyer, R. Tena-Zaera, V. Munoz-Sanjose, T. Frank, G. Pensl, Appl. Phys. A. **88**, 147 (2007)
43. Y. Natsume, H. Sakata, Mat. In Electronics **12**, 87 (2001)
44. Y. H. Shin, M. D. Kim, J. E. Oh, M. S. Han, S. G. Kim, K. S. Chung, J. Kor. Phys. Soc. **53**, 5 (2008)
45. K. Abe, M. Miura, M. Oiwa, J. Vac. Sci. Technol. A, **29**, 3 (2011)
46. C. Jagadish and J. Pearton, Zinc Oxide Bulk, Thin Films and Nanostructures Processing, Properties and Applications, Elservier, Oxford, UK, Amsterdam, Netherlands (2006)
47. S. M. Sze Physics of semiconductor devices, 2nd Edn. Wiley, New York (1981).
48. E. H. Rhoderick and R. H. Williams, Metal-semiconductor Contacts (Oxford University Press, Oxford 1988)
49. F. D. Auret, S. A. Goodman, G. Myburg, F. K. Koschnick, J.-M. Spaeth, B. Beaumont, and P. Gibart, Physica B, **273**, 84 (1999)
50. L. J. Brillson and Y. Lu, J. Appl. Phys. **109**, 121301 (2011)
51. B. G. Streetman, Solid State Electronic Devices, 5th Ed, Prentice Hall, New Jersey (2000)